Transaction B: Mechanical Engineering
Vol. 17, No. 1, pp. 13–24

SCIENTIA IRANICA

Effects of Unsteady Friction Factor on Gaseous Cavitation Model

M. Mosharaf Dehkordi[1] and B. Firoozabadi[1,*]

Abstract. *The condition known as a water-hammer problem is a transient condition that may occur as a result of worst-case loadings, such as pump failures, valve closures, etc. in pipeline systems. The pressure in the water hammer can vary in such a way that in some cases it may increase and cause destruction to the hydraulic systems. The pressure in the water hammer can also be decreased to the extent that it can fall under the saturation pressure, where cavitation appears. Therefore, the liquid is vaporized, thus, making a two-phase flow. This pressure decrease can be as dangerous as the pressure rise. As a result of the pressure drop and vaporization of the liquid, two liquid regions are separated, which is referred to as column separation. In almost all standard methods for simulation of column separation, the steady friction factor was used, but in reality, the quantity of the friction factor is variable. In this work, the unsteady friction factor has been applied in the Discrete Gas Cavity Model (DGCM), which is a standard method of column separation prediction. Through comparisons with experimental data, results showed that applying the unsteady friction factor can improve the magnitude of the predicted duration shape and the timing of the pressure pulse in all of the case studies.*

Keywords: *Water-hammer; Cavitation; Discrete gas cavity model; Unsteady friction model; Method of characteristics.*

INTRODUCTION

In a transient flow, a common concern of hydraulics engineers is to control the effect of the pressure wave, in order to protect relevant system components. Pressure waves are usually produced by the closure of a valve in simple systems. The pressure in hydraulic systems oscillates due to these pressure waves. In some cases, pressure reaches or drops below the vapor pressure and, therefore, cavitation occurs. Transient cavitation is an additional phenomenon accompanying the water-hammer. Cavitation can cause damage to the material of the pipes. The influence of a pressure rise due to cavitation and pressure oscillation caused by water-hammer can be harmful to a pipe wall, as well as to its fatigue life. In order to improve the performance and reliability of systems, it is important to predict the onset and degree of cavitation taking place [1]. Fluid mixtures in hydraulic systems can be classified into five groups:

1. Fully degassed liquid;
2. Fully degassed liquid with vapor;
3. Liquid with dissolved gas;
4. Liquid with dissolved and undissolved gas;
5. Liquid with dissolved and undissolved gas and vapor.

When the pressure reaches or drops below the vapor pressure of a liquid, the cavities grow very rapidly because of evaporation into the growing cavity. The process is called vaporous cavitation [1].

Cavitation can have a serious effect on pipeline systems. The accident at the Oigawa hydropower plant in 1950 in Japan is such an example, which was the result of column separation [2]. In that accident, three workers died. A fast valve-closure during maintenance caused an extreme high-pressure wave that split the penstock open. Therefore, a low pressure wave was generated causing cavitation and a portion of the pipeline was crushed due to the outer atmospheric pressure load. Jaeger et al. [3] reviewed the most serious accidents due to water-hammer and column separation. Many of the failures described were related to vibration and resonance [2].

1. *School of Mechanical Engineering, Sharif University of Technology, Tehran, P.O. Box 11155-956, Iran.*
*. *Corresponding author. E-mail: firoozabadi@sharif.edu*

Received 17 July 2008; received in revised form 20 May 2009; accepted 12 October 2009

In most industrial systems, a negligible amount of free and released gas in the liquid is assumed during column separation [4]. Two distinct types of column separation can be considered. The first type is local vaporization with a large void fraction. A local vapor cavity may form in places such as a valve or in elevated regions of the pipe.

The second type of column separation is distributed vaporous cavitation. In this type of column separation, the cavities may be extended over long sections of the pipe; the void fraction for the mixture of liquid and liquid-vapor bubbles is close to zero. As soon as a rarefaction wave progressively drops the pressure in an extended region of the pipe to liquid vapor pressure, distributed vaporous cavitation occurs. The collapse of a discrete vapor cavity and the movement of the shock wave front into a distributed vaporous cavitation region condense the vapor back to liquid. In transient events, the pressure oscillates; therefore, the pipeline systems may experience combined water-hammer and cavitation effects [5-7]. Several system parameters, including the type of transient regime (rapid closure of the valve and turbine load rejection), pipeline system properties (pipe dimensions, profile and position of valves) and hydraulic characteristics (velocity, pressure head, pipe wall friction, properties of liquid and pipe walls) have important effects on the location and intensity of column separation; therefore, the modeling and laboratory testing of these phenomena are difficult. Practical implications of column separation led to intensive laboratory and field research, starting at the end of the 19th century [4]. There are several research undertakings on a simple reservoir-pipeline-valve system. They showed that, when the cavities collapse at the valve, the pressure rise may or may not exceed the Joukowsky pressure rise, and cavities may form at the boundary or along the pipe [2,4].

There are different methods for the simulation of cavitation and column separation one of which is the Discrete Vapor-Cavity Model (DVCM) that is used in most commercial software packages for water-hammer analysis (such as HAMMER7) for simulating transient events in pipelines involving water column separation. Since the introduction of DVCM by Streeter [8], the DVCM may have generated unrealistic pressure head spikes due to multicavity collapse. Kranenburg [9], Wylie and Streeter [7], Simpson and Bergant [10] and Brunone et al. [11] investigated the effects of multicavity collapse in column separation. In an effort to improve the performance of the DVCM, several models were introduced by Wylie and Streeter [7] and Bergant and Simpson [6] as an alternative to the discrete vapor-cavity model; Provoost and Wylie [12] introduced the discrete gas cavity model (DGCM).

In this paper, DGCM was modified by considering the unsteady friction factor, and the angle of the characteristic line in the Methods Of Characteristics (MOC) was corrected. The simulation was performed by a VC++ computer code, which can consider both steady and unsteady friction factors in the DGCM model.

Discrete Gas Cavity Model (DGCM)

As the pressure in the hydraulic system reaches or drops below the vapor pressure of the liquid, column separation occurs. As long as the pressure remains above the vapor pressure, with the absence of free gas in liquid, the wave speed remains constant. Whenever the pressure reaches or drops below the vapor pressure, vaporization occurs and the dynamic behavior of the system is changed; although the wave speed remains constant throughout the regions containing pure liquid [5].

There are several methods for simulating cavitation in transient events, such as the Discrete Vapor Cavity Model (DVCM) and the Discrete Gas Cavity Model (DGCM). In DGCM, for modeling the free gas distributed throughout the liquid in a homogeneous mixture, a free-gas lumped mass at computing sections is considered [5]. As a result of pressure variation, each isolated small volume of gas expands and contracts isothermally (for very small cavities). Between the computing sections, pure liquid is considered, and lumping the free gas at discrete locations has an effect on wave propagation speed that closely matches actual wave speed in the distributed mixture.

Unsteady Friction Models

The steady or quasi-steady friction terms are used in the standard water-hammer and column separation algorithms and software packages. For slow transient flows where the wall shear stress has a quasi-steady behavior, this assumption is reasonable. But, for rapid transients, experimental data have shown a significant difference when the computational results are compared to those of measurements [4]. The unsteady friction terms can be classified into six groups [13]:

1. The friction term is dependent on the instantaneous mean flow velocity, V;
2. The friction term is dependent on the instantaneous mean flow velocity, V, and instantaneous local acceleration, $\partial V/\partial t$;
3. The friction term is dependent on instantaneous mean flow velocity, V, instantaneous local acceleration, $\partial V/\partial t$, and instantaneous convective acceleration, $V\partial V/\partial X$.

4. The friction term is dependent on instantaneous mean flow velocity, V, and diffusion, $\partial^2 V/\partial x^2$.
5. The friction term is dependent on instantaneous mean flow velocity, V, and weights for the past velocity changes, $W(\tau)$ (Zielke model);
6. The friction term is based on the cross-sectional distribution of instantaneous flow velocity (2-D models).

The Zielke model [14] was analytically developed for the transient laminar flow. The unsteady part of the friction term is related to the weighted past velocity changes at the computational section. The Zielke model requires large computer storage, and several researchers have tried to improve computational efficiency and/or extend its application to transient turbulent flow conditions.

The Brunone's model [15] is used in this paper, which is related to instantaneous local acceleration, $\partial V/\partial t$, and instantaneous convective acceleration, $V\partial V/\partial x$.

MATHEMATICAL MODELS

Discrete Gas Cavity Model (DGCM)

In this scheme, it is assumed that between each computing section, there is pure liquid (without free gas) and a liquid phase with a constant wave speed occupying the computational reach. The Discrete Gas Cavity Model (DGCM) allows gas cavities to form at computational sections in the method of characteristics. The DGCM is based on water-hammer compatibility equations, the continuity equation for the gas volume, and the ideal gas equation (isothermal process). The gas is assumed to behave isothermally, which is valid for tiny bubbles. Large bubbles and column separation tend to behave adiabatically. Figure 1 shows a section of the pipeline with a concentrated gas volume at computing sections. The perfect gas law is used to determine the volume of a constant mass of free gas in each computing section, which can be written in the following expression:

$$p_g^* \, \forall_g = M_g R_g T = p_0^* \alpha_0 \forall, \tag{1}$$

in which T is temperature, M_g is mass of gas, R_g is gas constant, and α_0 is the void fraction at some reference pressure, p_0^*.

In most cases, we deal with free air in water. In these cases we use the hydraulic-grade line convenient (Figure 1).

$$p_g^* = \rho_l g(H - z - H_\nu), \tag{2}$$

in which the hydraulic-grade line elevation, H, and the elevation of the pipeline, z, are measured from the same reference datum. Since $\forall$, the volume of mixture in a pipeline reach is a constant, Equation 1 may be used to determine the volume of gas at each section for initial conditions and for each time step:

$$\forall_g' = \frac{p_0^* \alpha_0 \forall}{p_g^*} = \frac{C_3}{H - z - H_\nu}, \tag{3}$$

in which $C_3 = p_0^* \alpha_0 \forall / \rho_l g$.

Figure 2 shows a staggered grid of characteristics when the gas volume is at an interior section in the pipeline.

The equations needed to solve the variable at each time step are:

The C^+ compatibility equation:

$$H = C_P - B_P Q_{Pu}. \tag{4}$$

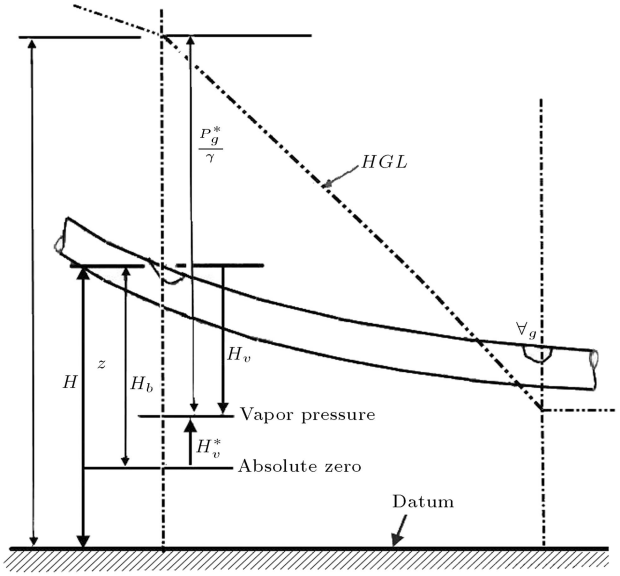

Figure 1. Hydraulic-grade line for the pipeline [5].

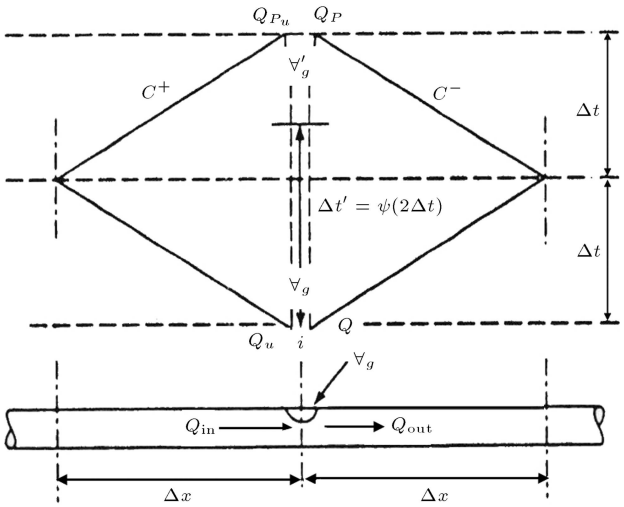

Figure 2. Staggered grid of characteristics at an interior section in the pipeline.

The C^- compatibility equation:

$$H = C_M - B_M Q_P, \tag{5}$$

in which the coefficients C_P, B_P, C_M and B_M are:

$$C_P = H_{i-1} - BQ_{i-1},$$

$$B_P = B + R|Q_{i-1}|,$$

$$C_M = H_{i+1} - BQ_{i+1},$$

$$B_M = B + R|Q_{i+1}|$$

in which $B = a/gA$ and $R = f\Delta x/2gDA^2$.

The continuity equation at the gas volume is:

$$\frac{d\forall_g}{dt} = Q_{\text{out}} - Q_{\text{in}}. \tag{6}$$

By using the weighting factor in the time direction (as shown in Figure 2), which is defined in the form:

$$\psi = \frac{\Delta t'}{2\Delta T}, \quad 0.5 < \psi \leq 1, \tag{7}$$

Equation 6 is integrated and yields:

$$\forall'_g = \forall_g + 2\Delta t \times [\psi(Q_P - Q_{Pu}) + (1-\psi)(Q - Q_u)], \tag{8}$$

in which $2\Delta t = 2\Delta x/a$ is time step, $\forall'_g$ and $\forall_g$ are gas volume at the current time and $2\Delta t$ earlier, respectively.

Substitution of Equations 4 to 6 into Equation 8 leads to:

$$(H - z - H_\nu)^2 + 2B_1(H - z - H_\nu) - C_4 = 0, \tag{9}$$

in which:

$$B_1 = -B_z(B_P C_M + C_P B_M) + B_2 B_P B_M B_\nu + (z + H_\nu)/2,$$

$$C_4 = C_3 B_P B_M B_2/(\Delta t\psi),$$

$$B_2 = 0.5/(B_M + B_P),$$

$$B_\nu = \lfloor \forall_g/(2\Delta t) + (1-\psi)(Q - Q_u)\rfloor/\psi.$$

This standard quadratic equation has the solution:

$$H - z - H_\nu = -B_1(1 + \sqrt{1 + B_B}) \quad \text{if} \quad B_1 < 0, \tag{10}$$

$$H - z - H_\nu = -B_1(1 - \sqrt{1 + B_B}) \quad \text{if} \quad B_1 > 0, \tag{11}$$

in which $B_B = C_4/B_1^2$. Equations 5 and 6 are used to find Q_{Pu} and Q_P, and Equation 8 is used to find $\forall'_g$.

A straightforward linearization of these equations, for the condition of $|B_B| << 1$ is used to avoid yielding inaccurate results due to inaccuracies in the numerical evaluation of the radical.

$$H - z - H_\nu = -2B_1 - \frac{C_4}{2B_1} \quad \text{if} \quad B < 0, \tag{12}$$

$$H - z - H_\nu = \frac{C_4}{2B_1} \quad \text{if} \quad B_1 > 0. \tag{13}$$

Thus, Equations 12 and 13 are used when $|B_B|$ is small (less than 0.001), and Equations 10 and 11 are used in all other cases.

To control the numerical oscillations that appear during the simulation of a transient, the weighting factor, ψ, is used [5]. Although the weighting factor, ψ, can take on values between 0 and 1.0, a practical range is 0.5-1.0. For values less than 0.5, the results are unstable, and at $\psi = 1$ there is minimum numerical oscillation [5].

Bergant et al. [16] showed that the value of void fraction, α_0, has significant effects on the pressure wave shape and timing for a very low gas void fraction; the DGCM model results perfectly matched with the results of standard water hammer model (in the absence of cavitation) It is also depicted that larger amounts of free gas have more effect on results in shape and timing. Therefore, the DGCM model can be successfully used for simulation of vaporous cavitation by utilizing a very low gas void fraction ($\alpha_0 \leq 10^{-7}$). Another factor that has a serious effect on results in shape and timing is the flow situation. Bergant considered two distinct flow situations:

1. Distributed free gas at all computational sections;
2. A trapped gas pocket at the midpoint of the pipeline system (shown in Figure 3). In the present work, DGCM was used by considering a very low gas void fraction and distributed free gas at all computational sections.

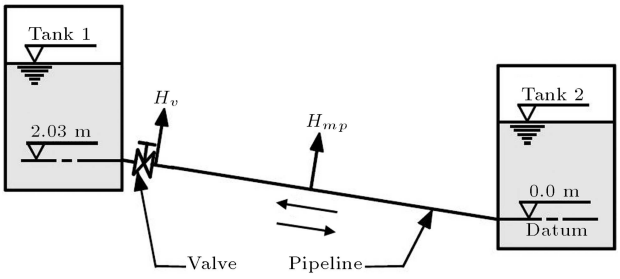

Figure 3. Schematic diagram of the test case [4].

Unsteady Friction Factor Models

In most software packages, the steady state friction factor is used for water-hammer analysis. For considering the effects of unsteady friction on water-hammer or column separation, friction factor f in Equations 4 and 5 can be expressed as the sum of a quasi-steady part, f_q, and an unsteady part, f_u, i.e. $f = f_q + f_u$. It should be mentioned that by setting $f_u = 0$ the steady friction model, f_q, is computed by updating the Reynolds number at each new computation, based on Vakil and Firoozabadi [13], who used an unsteady friction factor in water-hammer without cavitation.

Here, the Brunone model was used to consider the unsteady friction factor. The Brunone model relates the unsteady friction part, f_u, to the instantaneous local acceleration, $\partial V/\partial t$, and instantaneous convective acceleration, $V\partial V/\partial x$; Vitkovsky deduced a new formulation based on Brunone's model [15]:

$$f = f_q + \frac{k\ D\ A}{Q|Q|}\left(\frac{\partial Q}{\partial t} + a\ \mathrm{sign}(Q)\left|\frac{\partial Q}{\partial x}\right|\right), \qquad (14)$$

in which:

$$\mathrm{sign}(Q) = \{+1 \text{ for } Q \geq 0 \text{ and } -1 \text{ for } Q < 0\}.$$

The Brunone friction coefficient k can be predicted either empirically or analytically [17]. The analytical definition of k using Vardy and Brown's shear decay coefficient, C^*, is used in this paper:

$$k = \frac{\sqrt{C^*}}{2}, \qquad (15)$$

in which:

$$C^* = \begin{cases} 0.00476 & \text{for laminar flow} \\ \frac{7.41}{\mathrm{Re}^{\log(14.3/\mathrm{Re}^{0.05})}} & \text{for turbulent flow.} \end{cases} \qquad (16)$$

A first-order approximation for the friction term, i.e. $f.Q_{t-\Delta t}|Q_{t-\Delta t}|.\Delta x/(2gDA^2)$, is used in Equations 4 and 5 when using the Brunone model.

Characteristic Equation in DGCM with Unsteady Friction Term

Water hammer equations include the continuity equation and equations of motion with assumptions, such as one-dimensional flow, steady friction term and no-column separation. Neglecting small terms in comparison with other terms are as follows [17]:

$$L_1 = \frac{\partial H}{\partial t} + \frac{a^2}{gA}\frac{\partial Q}{\partial x} = 0, \qquad (17)$$

$$L_2 = \frac{\partial H}{\partial x} + \frac{1}{gA}\frac{\partial Q}{\partial t} + \frac{fQ|Q|}{2gDA^2} = 0. \qquad (18)$$

For considering the effects of unsteady friction in DGCM, substitution of Equation 14 into Equation 18 leads to:

$$L_2 = \frac{\partial H}{\partial x} + \frac{1}{gA}\frac{\partial Q}{\partial t} + \frac{f_q\ Q|Q|}{2gDA^2} + k\left(\frac{\partial Q}{\partial t} + a\ \Phi_A\ \frac{\partial Q}{\partial x}\right), \qquad (19)$$

in which:

$$\Phi_A = \begin{cases} -1 & \text{for} \quad Q\partial Q/\partial x < 0 \\ +1 & \text{for} \quad Q\partial Q/\partial x > 0 \end{cases}$$

Equations 2 and 12 are combined linearly using unknown multiplier λ in the form of $L_2 + \lambda L_1 = 0$, and using a material derivative for $H(x,t)$ and $Q(x,t)$ which leads to:

$$\frac{dx}{dt} = \frac{1}{\lambda} = \frac{a\Phi_A k + a^2\lambda}{1+k}, \qquad (20)$$

Equation 20 is solved for an unknown multiplier:

$$\lambda_{1,2} = \frac{-k\Phi_A}{2a} \pm \frac{1}{2a}(k+2). \qquad (21)$$

The procedure is similar to the MOC in a standard water-hammer, thus, by integrating along characteristic lines, the finite difference equation is determined. Considering the value of λ shows that, by using the unsteady friction coefficient, the angle of characteristic lines is changed and, thus, coefficients C_P, B_P, C_M and B_M are changed and must be updated. By using recent values of these coefficients, Equations 5 to 14 are computed.

Updating Brunone Friction Coefficient *k*

The analytical definition of k using Vardy and Brown's shear decay coefficient, C^*, that is used in this paper, is shown in Equations 15 and 16. In the present work, the Reynolds number is determined by using the local discharge in each computing section (node). However, in cases of cavitation, there are two local discharges in each computing section (inflow and outflow) and, therefore, there are two distinct methods for updating the local Reynolds number and the Brunone friction coefficient. With respect to the two forms of definition of the Vardy shear decay coefficient (Equation 16), whenever the local Reynolds number is not zero, the Brunone coefficient is updated. Both of these methods were studied. In Equation 19, Φ_A was introduced as follows:

$$\Phi_A = \begin{cases} -1 & \text{for} \quad Q\partial Q/\partial x < 0 \\ +1 & \text{for} \quad Q\partial Q/\partial x > 0 \end{cases}$$

To determine Φ_A, $Q\partial Q/\partial x$ must be calculated at each computing section, thus along the C^+ characteristic line:

$$(Q_u)_{i,t}.\frac{(Q_u)_{i,t} - Q_{i-1,t}}{\Delta x}, \tag{22}$$

and along the C^- characteristic line:

$$Q_{i,t}.\frac{(Q_u)_{i+1,t} - Q_{i,t}}{\Delta x}. \tag{23}$$

TEST CASE

To verify the present model, results were compared with the experimental data, as well as with other numerical results of column separation simulation in hydraulic systems.

Bergant and Simpson [4] designed and constructed flexible laboratory apparatus for investigating water hammer and column separation events in pipelines. Their apparatus is comprised of a straight sloping copper pipe connecting two pressurized tanks (Figure 3). The pipe slope is constant at 5.45% [4]. Water hammer events in the apparatus are initiated by rapid closure of the ball valve. The properties of this system are shown in Table 1.

RESULTS AND DISCUSSION

Different Initial Velocities

Results for two distinct flow velocities in an upward sloping pipe (shown in Figure 3; $V_0 = 0.3$ or 1.4 m/s) and a constant upstream end reservoir head (Tank 2; $H_{T,2} = 22.0$ m) are presented here. The numerical prediction and measured piezometric heads at the downstream end valve, $H_{\nu,1}$, and at the mid-point, H_{mp}, (Figure 3) were calculated for a low-velocity case ($V_0 = 0.3$ m/s). A comparison between experimental results [4] and the present work for the steady and unsteady friction DGCM can be seen in Figures 4 and 5, respectively.

Table 1. Properties of the system.

Internal Diameter	Pipeline Length	Upstream Head	Pipe Slope
0.0221 m	37.23 m	22 or 12 m	5.45%
Pipeline Elevation	**Steady Velocity**	**Downstream Valve Closure Time**	**Wave Speed**
2.03 m	0.3 m/s	0.009 s	1319 m/s

It should be mentioned that Equations 15 and 16 show that the Brunone friction coefficient depends on Reynolds number. In case of cavitations, there are two flows in each computational node (inflow and outflow), therefore, there are two different methods (two Reynolds numbers) for updating k in the unsteady friction model. In Figures 5 to 7, k in each node is updated by using the outflow.

The valve closure generates the water-hammer head, $H_{\nu,1} = 62.5$ m, and subsequent column separation at the valve in a time of 0.0662 seconds. The maximum measured head, $H_{\max;\nu,a} = 95.6$ m, occurs in a time of 0.1842 seconds as a narrow short-duration pressure pulse. The magnitude of the short-duration pressure pulse predicted by DGCM is $H_{\max;\nu,1} = 100.36$ m (present work: steady friction) and $H_{\max;\nu,1} = 101.9$ m from Bergant and Simpson simulations [4]. The unsteady friction DGCM (present work) pressure is predicted as $H_{\max;\nu,1} = 100.1$ m. A comparison of the results of all studied models and experimental results [4] is shown in Table 2. A comparison of pressure heads and times of occurrence is done for 4 points (these points are shown in Figure 4a).

As can be seen from Table 2, at all points the unsteady friction DGCM predicted by the present work has good agreement with the measured values reported by [4]. It is also evident that the unsteady friction model can improve the time and shape of oscillations.

Figure 6 shows a comparison between the present work and measured values of the downstream valve head for an inlet velocity of $V_0 = 1.4$ m/s. The maximum head at the valve is the water hammer head generated at a time of $2L/a$ after valve closure. The water hammer head predicted by DGCM (steady friction and unsteady friction terms) matches the measured head. In this case, using an unsteady friction term can predict a better result in shape and timing compared with the steady friction term.

Different Reservoir Static Heads

The results for two different static heads in the upstream end reservoir ($H_{T,2} = 12.0$ or 22.0 m) and initial velocity ($V_0 = 0.3$ m/s) are compared in Figures 4 to 7. A valve closure for $H_{T,2} = 12.0$ m generates column separation with a wide short-duration pressure pulse (Figure 7), which is compared to column separation with a narrow short- duration pressure pulse (Figures 4 and 5). The decrease of static head at the identical initial flow velocity results in the reduced amplitude of a short-duration pressure pulse (lower amplitude reservoir wave) and more intense cavitation [4]. Both numerical models accurately predict the magnitude of the wide short duration pressure pulse and the duration of the first cavity at the valve in comparison with the

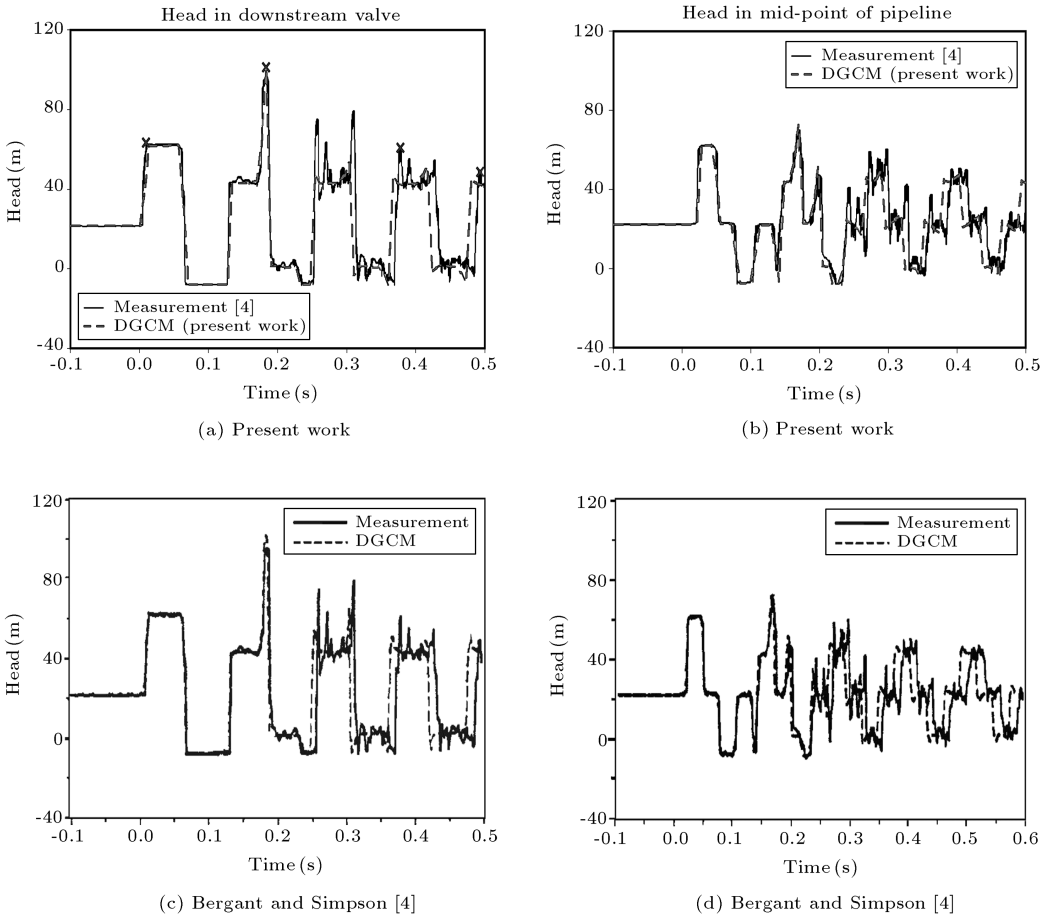

Figure 4. Comparison between measurements [4] and DGCM, with steady friction term.(a) and (b) Present Work, (c) and (d) Bergant and Simpson's work [4] ($V_0 = 0.3$ m/s).

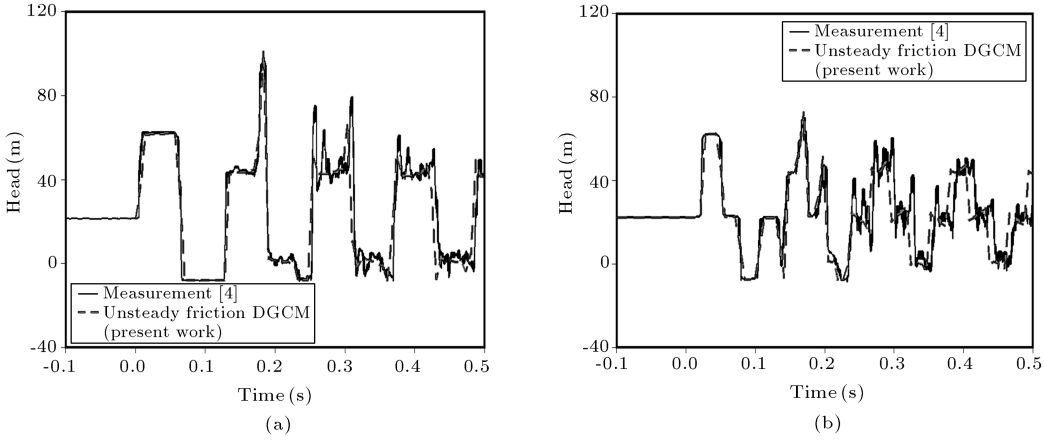

Figure 5. Comparison between present work (unsteady friction DGCM) and measured results ($V_0 = 0.3$ m/s). (a) Heads in downstream valve; (b) Mid-point of pipeline.

experimental data (Figures 7). As can be seen, the unsteady friction factor improves the results in the shape and timing of oscillations.

As shown in Table 3, the unsteady friction DGCM has better prediction than the DGCM model in agreement with measurement data [4].

Different Methods for Updating Brunone Friction Coefficient

In this work, the Brunone coefficient, k, is updated by using the local Reynolds number. In each node, as cavitation occurs, there are two different discharges

Table 2. Comparison of water-hammer head, maximum head, peak head, and time corresponding to peaks calculated from different numerical models and experimental data in downstream valve.

Point No. (as Shown in Figure 4a)	**1**		**2**		**3**		**4**	
Method of Evaluation	$H_{\nu,1}$ **(m) (1st Peak)**	**Time (s)**	$H_{\max;\nu,1}$ **(m) (2nd Peak)**	**Time (s)**	$H_{\nu,1}$ **(m) (4th Peak)**	**Time (s)**	$H_{\nu,1}$ **(m) (5th Peak)**	**Time (s)**
Measured Values [4]	62.50	0.0662	95.6	0.1842	60.51	0.3794	48.82	0.4945
Simulation DGCM [4]	62.42	0.0591	101.9	0.1833	51.339	0.3661	51.03	0.4792
DGCM with Steady Friction (Present Work)	62.43	0.0585	100.36	0.1834	46.174	0.3669	44.96	0.4798
DGCM with Unsteady Friction (Present Work)	62.43	0.0621	100.1	0.1841	55.84	0.3739	48.71	0.4868

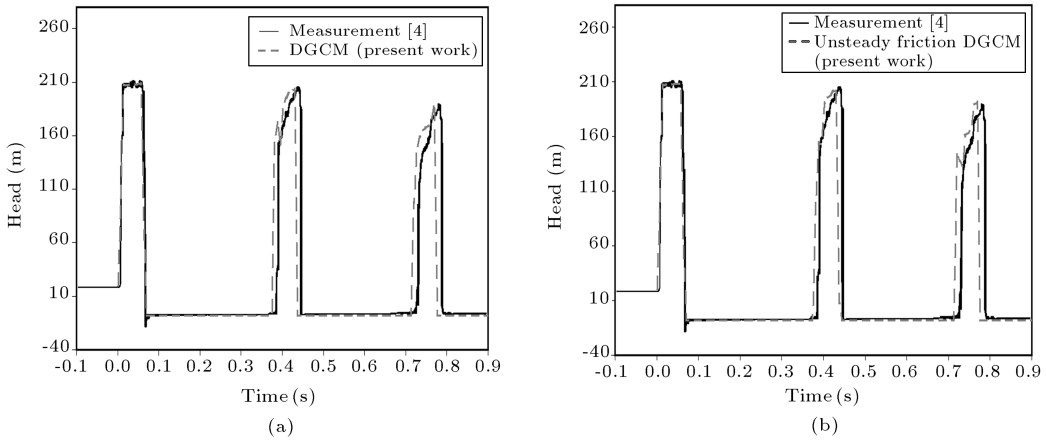

Figure 6. Comparison of heads in downstream valve for DGCM (a) and unsteady friction DGCM (b) with measured results ($V_0 = 1.4$ m/s).

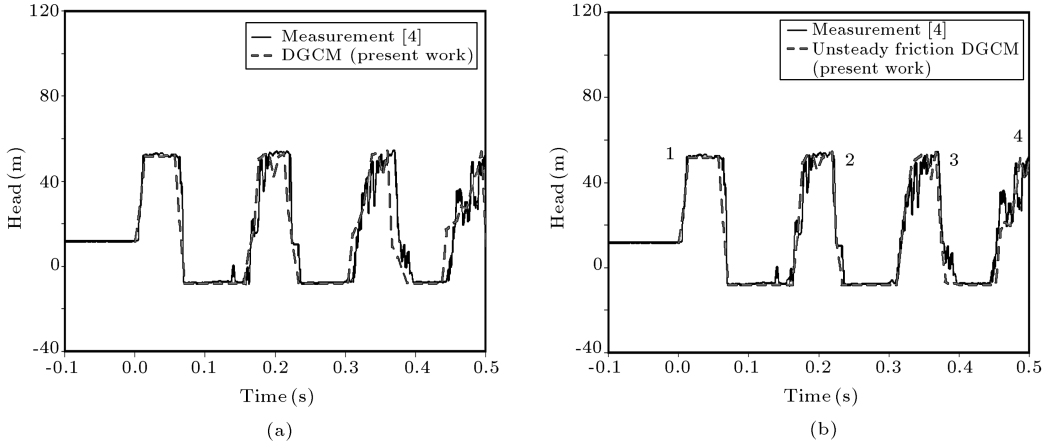

Figure 7. Heads in downstream valve; comparison between measured results [4] and predicted values by the present work. (a) Steady friction DGCM; (b) Unsteady friction DGCM; $H_{T,2} = 12.0$ m.

Table 3. Comparison of peak head, and time corresponding to peaks calculated from different numerical models and experimental data in downstream valve, $H_{T,2} = 12.0$ m.

Point No. (as Shown in Figure 4a)	**1**		**2**		**3**		**4**	
Method of Evaluation	$H_{\nu,1}$ **(m) (1st Peak)**	**Time (s)**	$H_{\nu,1}$ **(m) (2nd Peak)**	**Time (s)**	$H_{\nu,1}$ **(m) (3rd Peak)**	**Time (s)**	$H_{\nu,1}$ **(m) (4th Peak)**	**Time (s)**
Measured Values [4]	51.73	0.0135	53.48	0.2181	54.25	0.370	48.60	0.481
DGCM with Steady Friction (Present Work)	51.62	0.0141	53.16	0.2116	53.95	0.359	53.50	0.494
DGCM with Unsteady Friction (Present Work)	51.62	0.0141	54.07	0.2187	53.99	0.367	51.20	0.487

Q_{in} and Q_{out} (as shown in Figure 2), so the Reynolds number, $\text{Re} = VD/\nu = 4Q/\pi D\nu$, can be calculated using two different velocities. Therefore, there are two different methods for updating the Reynolds number.

In the first method, the Brunone coefficient, k, was updated, using the outflow of each node for calculation of the Reynolds number. In the second method, the local Reynolds number and the Brunone coefficient, k, were updated using inflow.

Figures 8, 9a and 10a show the results of unsteady friction DGCM (inflow) compared to the measurements [4] for a different initial velocity ($V_0 = 0.3$ or 1.4 m/s) and different upstream heads ($H_{T,2} = 12.0$ or 22.0 m).

Figures 9b, 10b and 11 show comparisons of all numerical models (that were studied) with measurements results. These figures show that using the unsteady friction model can improve the result, compared to the measurement, in most cases, but the form of applying the unsteady friction term in MOC and updating the Brunone coefficient are very important. In all conditions studied, unsteady friction DGCM (that uses outflow for calculation of the local Reynolds number) has had the best results (between all methods that were studied) compared to the measurement results; however, more studies are required to show the validity of this statement.

Figures 9b, 10b and 11 show that in some cases, the unsteady friction model predicts higher pressure peaks compared to steady friction models, but in general, the results of unsteady friction models (both inflow and outflow) are better than those of the DGCM model in timing. The problem (prediction of higher peaks) in the outflow model is less than that of the inflow model; therefore, the unsteady friction DGCM (using outflow for calculation of the local Reynolds number) is the best model for simulation of the column separation studies.

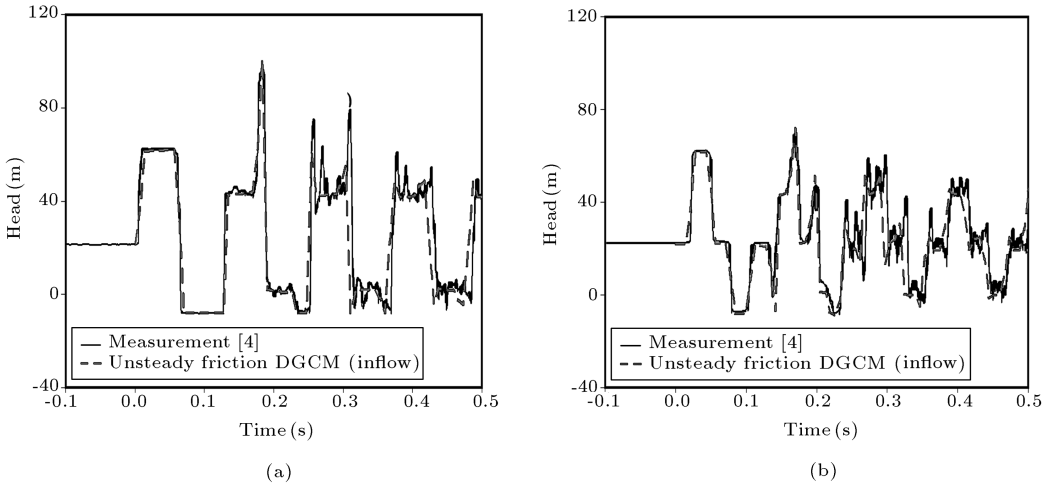

Figure 8. Comparison of heads for unsteady friction DGCM (inflow) (a) in downstream valve and (b) for mid-point of pipeline with measured results; $H_{T,2} = 22.0$ m, $V_0 = 0.3$ m/s.

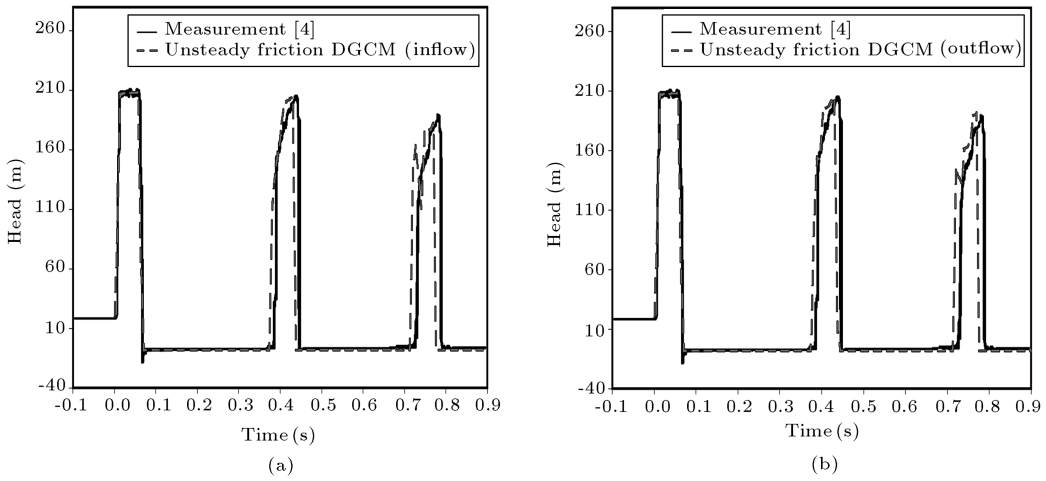

Figure 9. Comparison of heads in downstream valve for unsteady friction DGCM (inflow) (a) and all studied methods (b) with measured results; $H_{T,2} = 22.0$ m, $V_0 = 1.4$ m/s.

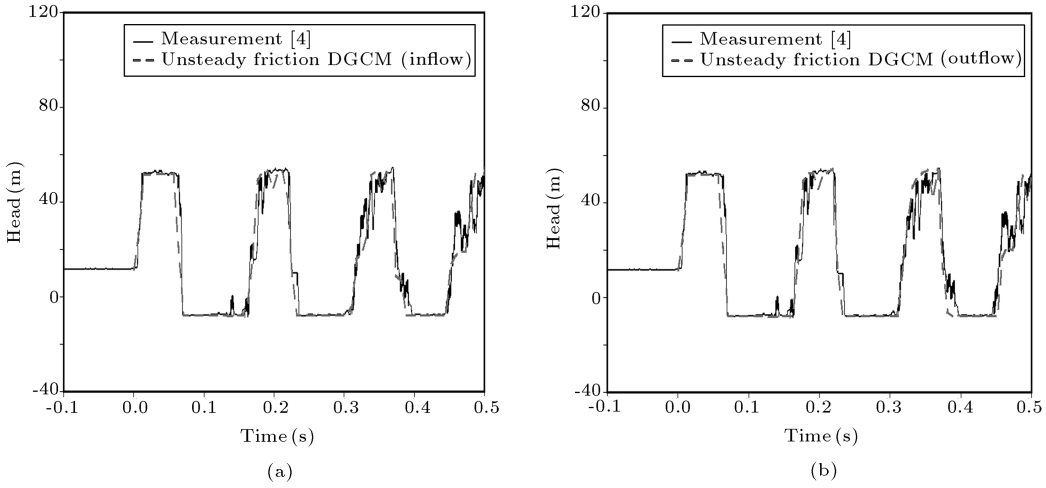

Figure 10. Comparison of heads in downstream valve for unsteady friction DGCM between inflow (a) and outflow (b) with measured results; $H_{T,2} = 12.0$ m, $V_0 = 0.3$ m/s.

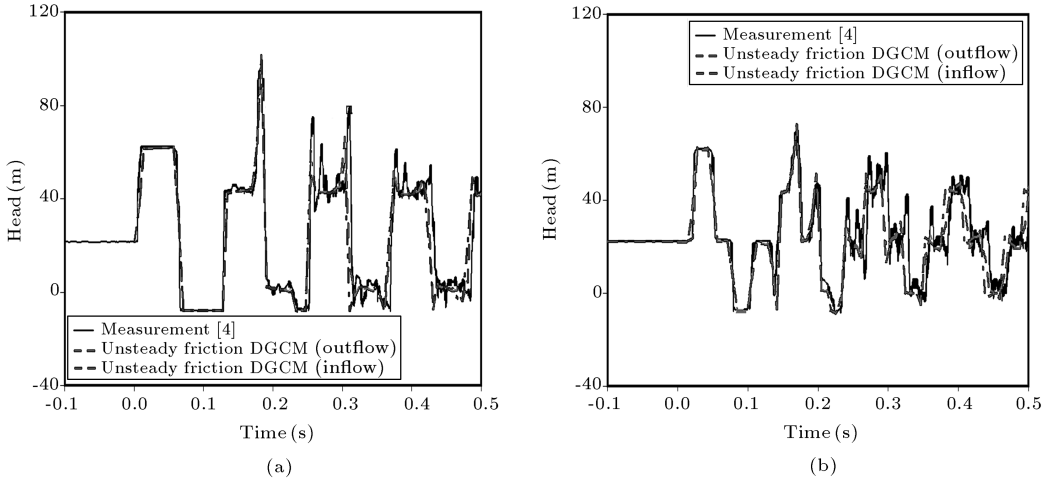

Figure 11. Comparison of heads for all studied methods (a) in downstream valve and (b) mid-point of pipeline with measured results; $H_{T,2} = 22.0$ m, $V_0 = 0.3$ m/s.

The velocity profiles have greater gradients in an unsteady condition, which results in higher energy dissipation compared with the steady condition. The results show that the unsteady friction factor has some fluctuations after the occurrence of each pressure peak, especially peak numbers 2, 3 and 4, which are shown in Figure 4a. Furthermore, in each time the values of the unsteady friction term are higher than the steady term, which is why it can predict a better agreement with experimental data. As far as we are concerned, the sound velocity and friction factor between two adjacent nodes are assumed to be constant; in other words, although there may be several friction factors, the friction factor between two adjacent computational nodes is constant. Figure 12 can clarify this point.

Finally, mesh independency was investigated and the results were independent of grid size.

CONCLUSION

The performance of the Brunone unsteady friction model has been tested for the DGCM for simulation of simple reservoir-pipeline-valve systems, including a test case. A comparison of two variations of the discrete vapor cavity model has been presented. The example presented shows that an unsteady friction model (modified Brunone's model) is able to predict a better result compared with measurements. These results clearly indicate the dependence of k on the Re number and the form of updating of this coefficient on the shape of the results. The modification of k with the local Reynolds number is the key to producing an improved prediction for two-phase transient flows. Further work is required to establish an appropriate k particularly for a case of two-phase flow.

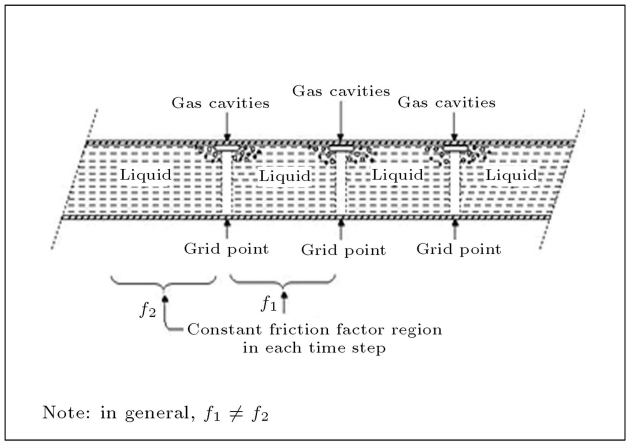

Figure 12. The variations of friction factors in pipeline in each time step.

NOMENCLATURE

a	water hammer wave speed
A	pipe area
C^+	positive characteristic equation
C^-	negative characteristic equation
C^*	Vardy's shear decay coefficient
D	pipe diameter
f_q	Darcy-Weisbach friction factor
g	gravitational acceleration
$\bar{H}$	barometric head
H_i	piezometric head
H_ν	vapor pressure head
k	Brunone's friction coefficient
L	pipe length
N	number of reaches in pipeline
Q	discharge at downstream side of computational section
Q_u	discharge at upstream side of computational section
p_0^*	reference pressure
p^*	absolute pressure
Re	Reynolds number VD/ν
T_c	valve closure time
V	flow velocity or velocity at downstream side of vapor cavity
V_{cav}	vapor cavity volume
Z_i	elevation of pipe section
λ	multiplier in characteristics method
ρ	liquid density
Δt	time step
Δx	reach length
Ψ	weighting factor

Subscripts

i	node number
mp	mid-point node

Abbreviations

DVCM	Discrete Vapor Cavity Model
MOC	Method Of Characteristics

REFERENCES

1. Shu, J.J. "Modeling vaporous cavitation on fluid transients", *International Journal of Pressure Vessels and Piping*, **80**, pp. 187-195 (2003).
2. Bergant, A. and Simpson, A.R. "Water hammer with column separation: A historical review", *Journal of Fluids and Structures*, **22**, pp. 135-171 (2006).

3. Jaeger, C., Kerr, L.S. and Wylie, E.B. "Water hammer effects in power conduits", *Proceedings of the International Symposium on Water Hammer in Pumped Storage Projects*, ASME Winter Annual Meeting, Chicago, USA, pp. 233-241 (1965).
4. Bergant, A. and Simpson, A.R. "Pipeline column separation flow regimes", *ASCE Journal of Hydraulic Engineering*, **125**(8), pp. 835-848 (1999).
5. Wylie, E.B. and Streeter, V.L., *Fluid Transients in Systems*, Prentice-Hall, Englewood Cliffs (1993).
6. Simpson, A.R. and Bergant, A. "Numerical comparison of pipe column-separation models", *ASCE, Journal of Hydraulic Engineering*, **120**, pp. 361-377 (1994).
7. Wylie, E.B. and Streeter, V.L. "Column separation in horizontal pipelines", *Proceedings of the Joint Symposium on Design and Operation of Fluid Machinery*, **1**, IAHR/ASME/ASCE, Colorado State University, Fort Collins, USA, pp. 3-13 (1978).
8. Streeter, V.L. "Transient cavitating pipe flow", *ASCE Journal of Hydraulic Engineering*, **109**(HY11), pp. 1408-1423 (1983).
9. Kraneburg, C. "Transient cavitation in pipelines", Ph.D. Thesis, Delft University of Technology, Dept. of Civil Engineering, Laboratory of Fluid Mechanics, Delft, The Netherlands (1974).
10. Simpson, A.R. and Bergant, A. "Developments in pipeline column separation experimentation", *IAHR, Journal of Hydraulic Research*, **32**, pp. 183-194 (1994).
11. Brunone, B., Golia, U.M. and Greco, M. "Effects of two-dimensionality on pipe transients modeling", *Journal of Hydraulic Engineering*, **121**(12), pp. 906-912 (1995).
12. Proovost, G.A. and Wylie, E.B. "Discrete gas model to represent distributed free gas in liquids", *Proceedings of the Fifth International Symposium on Water Column Separation*, IAHR, Obernach, Germany, Also: Delft Hydraulics Laboratory, Publication No. 263 (1982).
13. Vakil, A. and Firoozabadi, B. "Effect of the unsteady friction models and friction-loss integration on the transient pipe flow", *Scientia Iranica*, **13**(3), pp. 245-254 (2006).
14. Zielke, W. "Frequency-dependent friction in transient pipe flow", *Journal of Basic Engineering*, **90**(1), pp.109-115 (1968).
15. Brunone, B., Karney, W., Mecarelli, M. and Ferrante, M. " Velocity profiles and unsteady pipe friction in transient flow", *Journal of Water Resources Planning and Management*, **126**(4), pp. 236-244 (2000).
16. Bergant, A., Vithovsky, J. and Simpson, A.R. "Developing in unsteady pipe flow friction modeling", *Journal of Hydraulic Research*, **39**(3), pp. 249-257 (2001).
17. Bergant, A. and Simpson, A.R. "Cavitation inception in pipeline column separation", *Proceedings of the 28th IAHR Congress*, Graz, Austria, CD-ROM (1999).